Effects of coupled bichromatic atom-cavity interaction in the cavity-QED microlaser

Citation: Hong, Hyun-Gue et al. "Effects of coupled bichromatic atom-cavity interaction in the cavity-QED microlaser." Physical Review A 79.3 (2009): 033816. © 2009 The American Physical Society.

As Published: http://dx.doi.org/10.1103/PhysRevA.79.033816

Publisher: American Physical Society

Persistent URL: http://hdl.handle.net/1721.1/51751

Version: Final published version: final published article, as it appeared in a journal, conference proceedings, or other formally published context

Effects of coupled bichromatic atom-cavity interaction in the cavity-QED microlaser

Hyun-Gue Hong,[1] Wontaek Seo,[1] Moonjoo Lee,[1] Younghoon Song,[1] Wonshik Choi,[2] Christopher Fang-Yen,[2] Ramachandra R. Dasari,[2] Michael S. Feld,[2] Jai-Hyung Lee,[1] and Kyungwon An[1,*]

[1]*Department of Physics and Astronomy, Seoul National University, Seoul 151-742, Korea*

[2]*G. R. Harrsion Spectroscopy Laboratory, Massachusetts Institute of Technology, Cambridge, Massachusetts 02139, USA*

(Received 29 September 2008; published 13 March 2009)

In the observation of multiple thresholds in the cavity-quantum electrodynamics microlaser there was deviation from the result predicted by uniform atom-cavity coupling theory, notably a frequency-pushing behavior. We analyze in the semiclassical limit the tilted injection of atoms, originally used to achieve a spatially uniform atom-cavity coupling, and show that the deviation originates from the interference between the induced dipole moments associated with two traveling-wave components of a standing-wave cavity mode. The criteria for sufficiently reduced interference and thus uniform atom-cavity interactions are derived in analytic considerations and verified by numerical calculation. Our analysis is well supported by experimental data.

DOI: 10.1103/PhysRevA.79.033816 PACS number(s): 42.50.Pq, 42.50.Gy, 42.55.−f

I. INTRODUCTION

The cavity-quantum electrodynamics (QED) microlaser, an optical analog of the micromaser [1], is one of the most fundamental systems in quantum optics. It amplifies light via coherent interaction between a small number of two-level atoms and a single cavity mode under the strong-coupling condition. The first operation of the microlaser successfully demonstrated lasing in the single atom level [2]. But spatially nonuniform atom-cavity coupling was unavoidable as in most cavity-QED experiments [3–6] employing a collimated atomic beam in the optical frequency region. Typically, the atomic beam width extends over hundreds of wavelengths inside the cavity mode. Soon it was realized that position dependence in the coupling strength can be removed in effect by tilting the atomic beam and incorporating Doppler-shifted traveling-wave-like interactions [7] at the expense of reducing the coupling strength to a half of its original maximum. With this scheme the microlaser has successfully witnessed sub-Poissonian photon statistics [8] and multiple thresholds [9], which are theoretically predicted features under the uniform atom-cavity coupling condition.

It was observed, however, that the mean photon number in the cavity as a function of the intracavity atom number deviates from the theoretical prediction based on the uniform atom-cavity coupling condition as the system approaches the higher threshold region [10]. In particular, the mean photon number versus cavity detuning curve at a fixed atom number appears as if Doppler-shifted resonances got farther away from the rest-atom resonance by tens of MHz (*frequency-pushing* effect). According to the uniform coupling theory, the cavity-tuning curve should look symmetric with respect to a Doppler-shifted resonance frequency. The mechanical effect is ruled out because the additional Doppler shift induced by the optical force is much less than the mean Doppler shift. There was speculation that this asymmetry might be due to bichromatic interaction of the two traveling-wave components of the cavity field with the atoms [9–11], but no quantitative explanation to this asymmetry has been put forth so far.

Bichromatic atom-field interaction is a well-studied subject of considerable interest in atomic physics and quantum optics. Usually two independent coherent fields with different frequencies interact with an atom near resonantly. A unique feature of the bichromatic atom-cavity interaction in the microlaser, which also imposes additional difficulties, is that the two fields are the two traveling-wave components of a single standing-wave cavity field, which grows and shrinks by coherent interaction with the atoms while the Rabi angles involved in this interaction can be much larger than unity.

In this paper we solve the problem semiclassically (i.e., mean photon number much greater than unity) by evaluating the unitary operator associated with the atom-cavity interaction in Dyson series with an explicit time-position-dependent atom-cavity coupling. We show that the frequency pushing originates from a bichromatic interference between the atomic dipoles induced by the two traveling-wave components. We also show the frequency pushing accompanies spatial nonuniformity in the atom-cavity interaction. We then find criteria to achieve uniform coupling regardless of the occurrence of multiple thresholds. In fact, the experimental condition of Ref. [9] does not meet the criteria strictly. Our experimental data strongly support the validity of the criteria while nicely fit by theoretical curves.

The phase sensitivity is often encountered in the problem of interaction between two-level atoms and bichromatic fields [12]. The previous relevant theories [13–15] are limited to small Rabi angles. The present work registers another progress on this subject by giving an insight on the influence of the detuning between bichromatic fields to phase sensitivity beyond the first-order effect.

A similar criterion on the Doppler shift (degree of atomic beam tilting) for achieving spatially uniform vacuum Rabi oscillation via unidirectional momentum transfer has been given in a quantum theory with the atomic center-of-mass motion quantized [16]. Our criteria may be regarded as its natural extension to the semiclassical limit. In addition, we derive our criteria analytically whereas the analogous criterion in Ref. [16] was found by numerical analysis. Furthermore, we present in detail the effect of interference and

*kwan@phya.snu.ac.kr

thereby the microlaser output if the criteria are not strictly met. As another previous study we also note that a quantum trajectory analysis of the correlation measurement in a cavity-QED setting was given for a misaligned atomic beam [17]. Although the degradation of nonclassical correlation due to Doppler shift was nicely explained, the notion of coupling between bichromatic components was not clear.

This paper is organized as follows. In Sec. II, a semiclassical theory to determine the steady-state solution of the microlaser is explained. We derive analytic expressions regarding the emission probability for a tilted atomic beam configuration in Sec. III and numerically calculate the microlaser output in Sec. IV. We present experimental results which strongly support our analysis with correct fits in Sec. V.

II. STEADY STATES UNDER UNIFORM COUPLING

Let us review how to determine the steady states of the microlaser assuming a uniform coupling. In the microlaser a stream of barium atoms traverses a high-Q (3×10^9) cavity mode. Atom-cavity coupling g, cavity decay rate Γ_c, and atomic spontaneous emission rate Γ_p are $2\pi\times$ (380, 150, 50) kHz, respectively, and thus the so-called strong-coupling condition, $2g \gg \Gamma_c, \Gamma_p$, is satisfied. The atoms are fully inverted to their excited states of $^1S_0$-$^3P_1$ transition before entering the cavity mode. Energy is delivered to the cavity according to an emission probability P_{em} determined by coherent atom-cavity interaction. The energy inflow thus equals atomic flux times the emission probability. Since the atomic decay during the transit time τ through the cavity mode is negligible $(\Gamma_p\tau \ll 1)$, the main mechanism to lose energy in this system is through the coupling to the outside continuum modes, which is phenomenologically designated as $\Gamma_c n$ regardless of atomic parameters. Then the mean photon number n in the steady state is determined by the so-called gain-loss equation

$$\frac{N}{\tau}P_{em} = \Gamma_c n, \tag{1}$$

where N is the mean number of atoms inside the cavity. The left-hand side of Eq. (1) is a gain of the microlaser whereas the right-hand side describes a loss. Self-consistent determination of the steady state via rate equations was first introduced in Ref. [18]. In the present many-atom system, the cross interaction between atoms can be neglected since the change in the Rabi angle induced by adding or subtracting a photon by the other atoms inside the cavity is very small when the mean photon number is much larger than unity [19]. The problem is then reduced to obtaining the emission probability as a function of n, τ, and cavity-atom detuning Δ.

The emission probability is obtained as follows. Let us denote the excited state a, the ground state b, and the frequency of each level as ω_a, ω_b, respectively. The dipole interaction with a light field of $E_0 \cos \omega t$ is described by a Hamiltonian

$$H = H_0 + H_1, \tag{2}$$

where

$$H_0 = \hbar\omega_a|a\rangle\langle a| + \hbar\omega_b|b\rangle\langle b| \tag{3}$$

and

$$H_1(t) = \hbar\Omega_0 \cos \omega t|a\rangle\langle b| + \text{H.c.}, \tag{4}$$

where $\Omega_0 = \mu E_0/\hbar$ is the Rabi frequency associated with E_0 and "H.c." stands for Hermitian conjugate. It is convenient to work in the interaction picture with

$$U_0(t) = \exp(-i\omega_a t)|a\rangle\langle a| + \exp(-i\omega_b t)|b\rangle\langle b|. \tag{5}$$

The transformed interaction Hamiltonian is then given by

$$V(t) = U_0^\dagger(t)H_1(t)U_0(t)$$
$$\simeq \frac{1}{2}\hbar\Omega_0[\exp(-i\Delta t)|a\rangle\langle b| + \exp(i\Delta t)|b\rangle\langle a|] \tag{6}$$

under the rotating wave approximation with $\Delta = \omega - (\omega_a - \omega_b) \equiv \omega - \omega_0$. The atomic ket state evolves by an unitary operator as

$$|\psi_I(\tau)\rangle = U_I(\tau)|\psi_I(0)\rangle = U_I(\tau)|a\rangle, \tag{7}$$

where $U_I(\tau)$ is a time evolution operator given by

$$U_I(\tau) = \exp\left[-\frac{i}{\hbar}\int_0^\tau V(t)dt\right], \tag{8}$$

and the emission probability is the given by $P_{em} = |\langle b|U_I(\tau)|a\rangle|^2$. The time evolution operator is explicitly expanded in Dyson series as

$$U_I(\tau) = 1 - \frac{i}{\hbar}\int_0^\tau V(t_1)dt_1 + \left(\frac{-i}{\hbar}\right)^2 \times \int_0^\tau \int_0^{t_1} V(t_1)V(t_2)dt_1dt_2 + \cdots, \tag{9}$$

where obviously only odd terms contribute to the transition amplitude $\langle b|U_I(\tau)|a\rangle$. It is well known [20]

$$\langle b|U_I(\tau)|a\rangle = \sum_{n=0}^{\infty}\left(\frac{-i\Omega_0}{2}\right)^{2n+1}\int_0^\tau dt_{2n+1}\int_0^{t_{2n+1}} dt_{2n}\cdots\int_0^{t_1} dt_1 \times \exp[i\Delta(t_{2n+1} - t_{2n} + \cdots - t_2 + t_1)]$$
$$= \frac{-i\Omega_0}{\sqrt{\Omega_0^2+\Delta^2}}\sin\left(\frac{\sqrt{\Omega_0^2+\Delta^2}\tau}{2}\right)\exp(-i\Delta\tau/2), \tag{10}$$

thereby

$$P_{em} = \frac{\Omega_0^2}{\Omega_0^2+\Delta^2}\sin^2\left(\frac{\sqrt{\Omega_0^2+\Delta^2}\tau}{2}\right). \tag{11}$$

If the Rabi frequency acquires an overall phase, say $\Omega_0 \rightarrow \Omega_0 \exp(ikz_0)$, the expression of the transition amplitude in Eq. (10) is also multiplied by the factor $\exp(ikz_0)$, which makes no physical difference in the emission probability.

Using the relation $\Omega_0 = 2g\sqrt{n}$, we obtain the expression for $P_{em}(\Delta, n; \tau)$. We can construct a map of gain on (Δ, n) space and the steady states are determined by intersection curves between the gain map and the plane of cavity decay $\Gamma_c n$ as shown in Fig. 1. For each closed curve, the lower half at

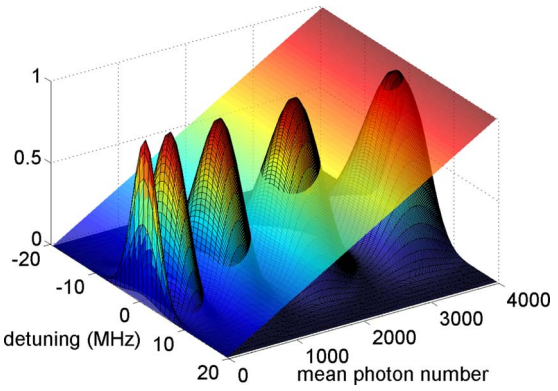

FIG. 1. (Color online) Illustration showing how the steady-state detuning curve is determined. There are five stable branch solutions in this case.

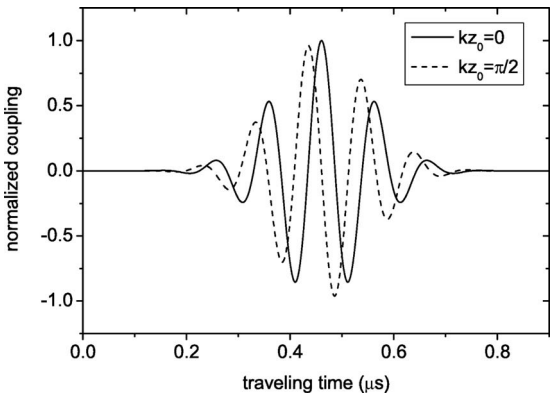

FIG. 2. Mode function for atoms injected into the cavity at two different positions ($kz_0=0,\pi/2$) with a tilt angle with Doppler shift of $\delta/2\pi=22.8$ MHz at a speed of $v=750$ m/s, which are typical experimental parameters.

which the slope of the gain along the photon number is positive constitutes an unstable solution, thus will not be considered [9]. The upper half of each curve is a part of a microlaser detuning curve, what is measured in a typical experiment, where the cavity's resonant frequency is scanned at a given input atomic flux. There are more than one set of solution if the atomic flux is high enough and we call the nth curve as nth branch solution. Since Eq. (11) is symmetric with respect to the sign of Δ the detuning curve is also expected to be symmetric.

III. EFFECT OF TILTED INJECTION OF ATOMS ON THE ATOM-CAVITY INTERACTION

If we tilt the atomic beam slightly, the atom's coordinate along the cavity axis is given by $z(t)=z_0+ut$, where z_0 is the position of injection for the specific atom and u is the velocity along the cavity axis. In a typical experiment the transverse velocity is $v=800$ m/s and the tilt angle is tens of mrad, thus u is order of 10 m/s and the corresponding Doppler shift $\delta(\equiv ku)/2\pi$ is order of 10 MHz. The mode function for a TEM_{00} Gaussian mode in the atomic frame of reference is

$$\cos(\delta t + kz_0)\exp[-(x^2+y^2)/w^2], \tag{12}$$

where x and y are the transverse coordinates orthogonal to z and w is the mode waist. Plots of the mode function for two representative values of kz_0 are shown in Fig. 2. Note that the incident position z_0 is mapped to the phase of amplitude modulation while it is mapped to the amplitude itself for normal injection ($\delta=0$).

Our model Hamiltonian in the tilted case is given by

$$H_1(t) = \hbar\Omega_0 \cos(\delta t + kz_0)\cos\,\omega t|a\rangle\langle b| + \mathrm{H.c.} \tag{13}$$

and the transformed interaction Hamiltonian $V(t)$ is, apart from $\hbar\Omega_0/2$,

$$\begin{aligned}&(\exp\{-i[(\Delta-\delta)t-kz_0]\}+\exp\{-i[(\Delta+\delta)t+kz_0]\})|a\rangle\langle b|\\&+(\exp\{i[(\Delta-\delta)t-kz_0]\}+\exp\{i[(\Delta+\delta)t+kz_0]\})|b\rangle\langle a|.\end{aligned} \tag{14}$$

Let us call the corresponding unitary operator $U_I^{\mathrm{tilt}}(\tau)$. For this bichromatic interaction a closed-form solution of $\langle b|U_I^{\mathrm{tilt}}(\tau)|a\rangle$ is not known to our knowledge. However we can get an insight on the interference between bichromatic components under a specific condition. For $\lambda\equiv\Omega_0\tau/2<1$, we may seek the first-order term of the Dyson series in λ, which is written as

$$\begin{aligned}&\frac{\{\exp[i(\Delta-\delta)\tau]-1\}}{i(\Delta-\delta)\tau}\exp(-ikz_0)\\&+\frac{\{\exp[i(\Delta+\delta)\tau]-1\}}{i(\Delta+\delta)\tau}\exp(ikz_0).\end{aligned} \tag{15}$$

Its contribution to P_{em} is then $\lambda^2\times$

$$\begin{aligned}&\mathrm{sinc}^2\left[\frac{(\Delta-\delta)\tau}{2}\right]+\mathrm{sinc}^2\left[\frac{(\Delta+\delta)\tau}{2}\right]\\&+2\cos\begin{pmatrix}\delta\tau\\+2kz_0\end{pmatrix}\mathrm{sinc}\left[\frac{(\Delta-\delta)\tau}{2}\right]\mathrm{sinc}\left[\frac{(\Delta+\delta)\tau}{2}\right].\end{aligned} \tag{16}$$

The expansion parameter $\lambda(=\sqrt{n}g\tau)$ has a meaning of the accumulated Rabi angle during τ in the presence of n photons. The first and second terms represent the interaction with the blueshifted and redshifted traveling waves, respectively, if $\delta>0$, and the third term represents the interference between them. Nonuniform feature or kz_0 dependence solely comes from the interference term. Figure 3 shows the difference of the cross term at an antinode ($kz_0=0$) and at a node ($kz_0=\pi/2$). The most dramatic difference arises for $|\delta\tau|<1$. For normal injection ($\delta\tau=0$) it simply states that the interaction is present there or not. We also observe that for the antinode the emission of photon is enhanced for $\Delta^2>\delta^2$ whereas it is enhanced for $\Delta^2<\delta^2$ for the node. To suppress the terms of spatial dependence we should then have

$$|\delta| \gg 1/\tau, \tag{17}$$

which indicates the separation of two Doppler-shifted resonance peaks should be much larger than the transit-time broadened width of each in the detuning curve.

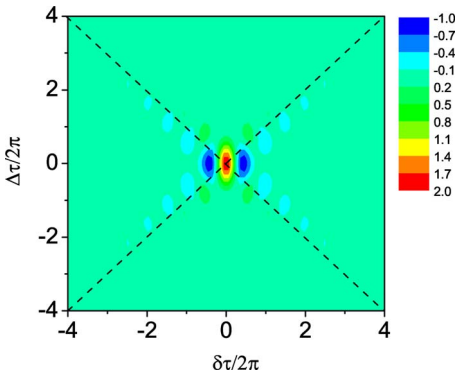

FIG. 3. (Color online) Density plot of the difference of the cross term for $kz_0=0$, $\pi/2$ as a function of $\Delta\tau$ and $\delta\tau$. Dashed lines $\Delta = \pm\delta$ are shown for comparison.

The typical experimental situation, however, cannot be fully understood by the first-order term only since $\lambda=\sqrt{n}g\tau \sim 1$ for $n\simeq 80$, which is then limited to the first branch solution. The next high-order terms are very complicated for arbitrary Δ. For clarity let us focus on the situation in which the cavity is tuned to one of the Doppler-shifted resonances, say, $\Delta=\delta$. The first-order term then reads $\lambda\times$

$$1+\mathrm{sinc}(\delta\tau/2)\exp[i(\delta\tau+2kz_0)] \tag{18}$$

apart from an overall phase. The interpretation is the same as given above for arbitrary Δ with the second term representing the interference between bichromatic components. The third-order term reads $\lambda^3\times$

$$\frac{1}{3!}+\frac{1-\cos(\delta\tau)\mathrm{sinc}(\delta\tau)}{2(\delta\tau)^2}+\frac{1}{2}\mathrm{sinc}(\delta\tau)\exp[i(\delta\tau+2kz_0)] + \frac{\cos(\delta\tau)\mathrm{sinc}(\delta\tau)}{2(\delta\tau)^2}\exp[-i(\delta\tau-2kz_0)] + \frac{1-\mathrm{sinc}(2\delta\tau)}{4(\delta\tau)^2}\exp[i(2\delta\tau+4kz_0)], \tag{19}$$

where the first term comprises clean Rabi oscillation since those terms are summed up as

$$\sum_{n=0}^{\infty}\frac{(-i\lambda)^{2n+1}}{(2n+1)!}=-i\,\sin(\lambda). \tag{20}$$

Here again we observe that the spatially nonuniform contribution with the kz_0 dependence contains $\mathrm{sinc}(\delta\tau)$ or powers of $(\delta\tau)^{-1}$, which falls rapidly as a function of $\delta\tau$. These envelopes are persistent to the terms other than those in Eq. (20) for even higher-order terms of Dyson series. Thus the criterion in Eq. (17) is still valid for the higher orders of λ. Another feature to note in the higher-order terms is the appearance of harmonic resonances such as $2\delta\tau, 3\delta\tau$, and so on.

As λ gets larger beyond unity, however, the kz_0-dependent terms and harmonic contributions get amplified. Thus we need to ultimately involve λ in the criterion for $\delta\tau$. The general condition for arbitrarily large λ is obtained as follows. Ideal Rabi oscillations with the coupling strength reduced to a half is expected if we achieve a spatially uniform and interference-free situation. In other words, on a Doppler-shifted resonance (say $\Delta=\delta$) the transition amplitude is very close to that given by Eq. (10) with $\Omega_0\rightarrow\Omega_0/2$ and $\Delta=0$ regardless of kz_0. Thus we calculate the remaining secondary terms other than the ideal Rabi oscillation in the transition amplitude as

$$\begin{aligned}
&\langle b|U_I^{\mathrm{tilt}}(\Delta=\delta)|a\rangle-\langle b|U_I(\Delta=0)|a\rangle_{\Omega_0\rightarrow(1/2)\Omega_0\exp(-ikz_0)}\\
&\quad=\exp(-ikz_0)\sum_{n=0}^{\infty}\left(\frac{-i\Omega_0}{4}\right)^{2n+1}\\
&\qquad\times\int_0^{\tau}dt_{2n+1}\int_0^{t_{2n+1}}dt_{2n}\cdots\int_0^{t_1}dt_1\\
&\qquad\times\{1+\exp[2i\delta(t_{2n+1}-t_{2n}+\cdots-t_2+t_1)]\\
&\qquad\times\exp(2ikz_0)-1\}\\
&\quad=\frac{-i\Omega_0\exp(ikz_0)}{\sqrt{(\Omega_0/2)^2+(2\delta)^2}}\sin\left(\frac{\sqrt{(\Omega_0/2)^2+(2\delta)^2}\,\tau}{2}\right)\exp(-i\delta\tau)
\end{aligned} \tag{21}$$

by using Eq. (10) and the arbitrariness of the overall phase in the Rabi frequency. Hence to suppress the magnitude of Eq. (21) another criterion for spatially uniform coupling can be generally declared as

$$|\delta|\gg\Omega_0/2. \tag{22}$$

With Eq. (17) we can then summarize as

$$|\delta|\gg\mathrm{Max}[\sqrt{n}g,1/\tau]. \tag{23}$$

The requirement of large Doppler shift for spatially uniform coupling is reminiscent of a similar criterion $|\delta|\gg g$ for clean vacuum Rabi oscillation in Ref. [16]. Both the present analysis and that of Ref. [16] deal with a similar situation where the position of the atomic beam along the standing wave is not determined but its momentum is well defined. In Ref. [16], the unidirectional momentum transfer occurs because the recoil to the other direction is effectively suppressed by a large detuning from the corresponding traveling-wave component. Although the momentum and the photonic quantum basis are not considered in the present semiclassical analysis, the underlying principle, that is, decoupling the opposite traveling-wave components by tilting the atomic beam is the same in both cases. As mentioned earlier in Sec. I, the extension to the semiclassical regime with $n\gg 1$ is given here analytically rather than by numerical observation.

Intuitively the frequency pushing can be understood as follows. In the higher branch solutions the atoms undergo more than one cycle of Rabi oscillation. The emitted photons are reabsorbed by the atoms several times there. Let us consider an excited atom, with a transverse velocity u along the cavity axis (z axis), emitting a photon in $+z$ direction at $\omega_0+\delta$ due to Doppler shift. The photon reflected back to the same atom then appears to be at $\omega_0+2\delta$, creating an induced dipole at that frequency. Further re-emission would then occur at $\omega_0+3\delta$ in $+z$ direction, and so on. Likewise, the emis-

sion in $-z$ direction would result in frequencies $\omega_0-\delta, \omega_0-3\delta$, etc. The interference between such multiphoton processes is the physical origin of the harmonic resonance which is also the very reason of the frequency pushing. Since both traveling-wave components are constituents of the same standing wave, the effect of the detuned traveling-wave component gets inevitably stronger as the Rabi frequency of the common cavity field grows. In Sec. IV, the correct effect of the traveling-wave interference in the microlaser signal is calculated for the first time.

IV. NUMERICAL RESULTS

A numerical method including the coupling between two traveling-wave components in the microlaser has been devised in Ref. [11]. The strategy is to divide the induced polarization of the atomic dipole into two parts, each of which corresponds to one of the traveling waves. The coupling between them are taken into account by considering a common cavity field operating on both atomic polarization. As we will show later in this section the approach in Ref. [11] is missing the harmonic resonances, and thus failed to explain the frequency pushing quantitatively.

Here we present the correct calculation for the frequency pushing and the related deviation from the uniform coupling theory by directly employing the amplitude-modulated mode function as in Eq. (12). Numerical integration of the optical Bloch equation is performed in order to obtain the emission probability. The equations are

$$\dot{S}_1(t) = \Delta S_2(t), \tag{24}$$

$$\dot{S}_2(t) = -\Delta S_1(t) + \Omega(t) S_3(t), \tag{25}$$

$$\dot{S}_3(t) = -\Omega(t) S_2(t), \tag{26}$$

where $2S_1(t)=\rho_{ab}\exp(i\omega t)+\rho_{ba}\exp(-i\omega t)$, $2S_2(t)=i[\rho_{ab}\exp(i\omega t)-\rho_{ba}\exp(-i\omega t)]$, $S_3(t)=\rho_{aa}-\rho_{bb}$, and $\Omega(t)$ is the Rabi frequency including the amplitude-modulated mode function. The emission probability is given by $\frac{1}{2}[1-S_3(\tau)]$ for the initial condition of $S_1(0)=S_2(0)=0$, $S_3(0)=1$. We present the results for two kinds of transverse envelope of $\Omega(t)$, a top hat and a Gaussian profile. The former is consistent with the analysis in the previous section and allows us to identify the contribution of kz_0-dependent terms in the emission probability. The latter is consistent with the experiment and will hence be used to explain the experimental results. The monoenergetic beam is assumed in order to clarify the essence of the physics although we take into account the inhomogeneous velocity broadening of the actual atomic beam when we give a fit to the experimental data in Sec. V.

A. Top-hat mode profile

Figure 4 shows the emission probability for four different tilt angles or Doppler shifts. The left column (a)–(d) is drawn for injection at the antinode and the right column (e)–(h) for the node. Doppler shift $\delta/2\pi$ is increased from 0 to 45 MHz. For normal injection, (a) and (e), P_{em}'s are very different

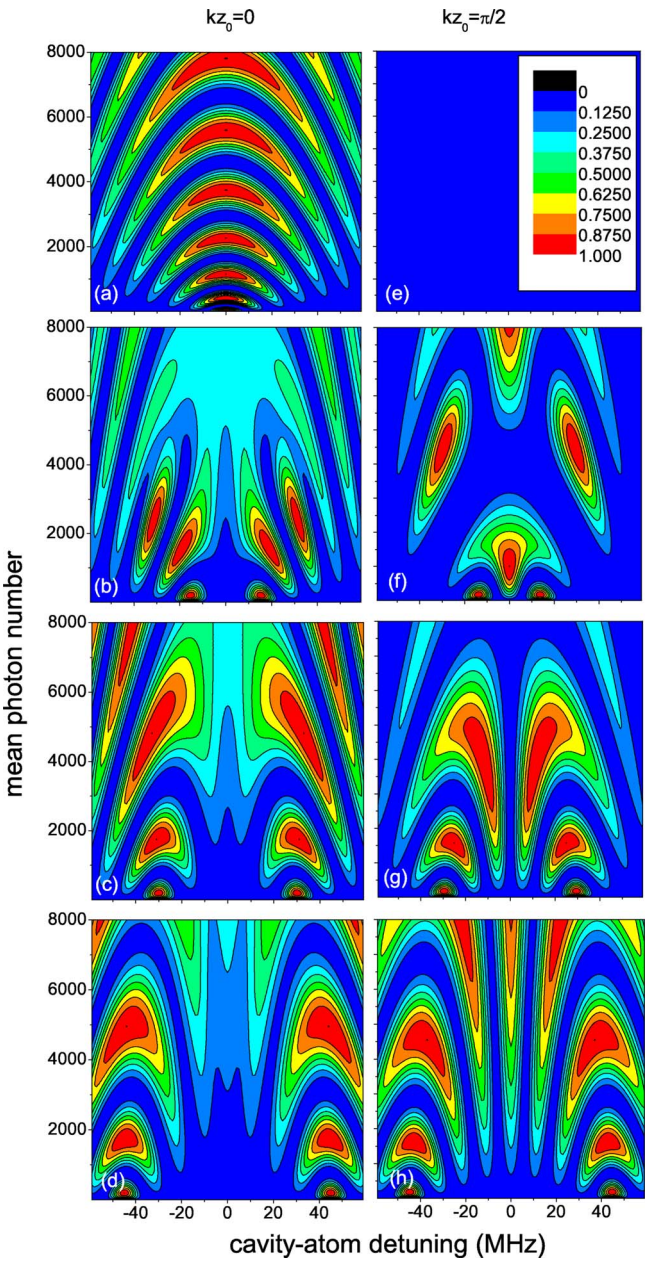

FIG. 4. (Color online) Density plots of emission probabilities for the antinode [(a)–(d)] and the node [(e)–(h)]. A top-hat mode profile is assumed. From the first row to the fourth, $\delta/2\pi$ are 0, 15, 30, and 45 MHz, respectively. Typical parameters in the experiment, $v=750$ m/s (monovelocity) with $g/2\pi=380$ kHz and $\Gamma_c/2\pi=150$ kHz, are used.

depending on the injection position z_0. It simply reflects the fact that Rabi frequency is largest at the antinode and no interaction at the node. For an intermediate tilt angle, (b) and (f), at which $\delta\simeq\sqrt{n}g$ at $n\simeq 6000$ a significant dependence on kz_0 emerges for $n>1000$. As expected, the interference effect comes into play in such a way that P_{em} reaches unity with smaller n for $|\Delta|>|\delta|$ for the antinode whereas it does for $|\Delta|<|\delta|$ for the node (recall the discussion on Fig. 3). Furthermore, we also find gain peaks roughly at the twice of δ in Fig. 4(f), which is identified as a harmonic resonance which appears in the higher-order expansion of Dyson series.

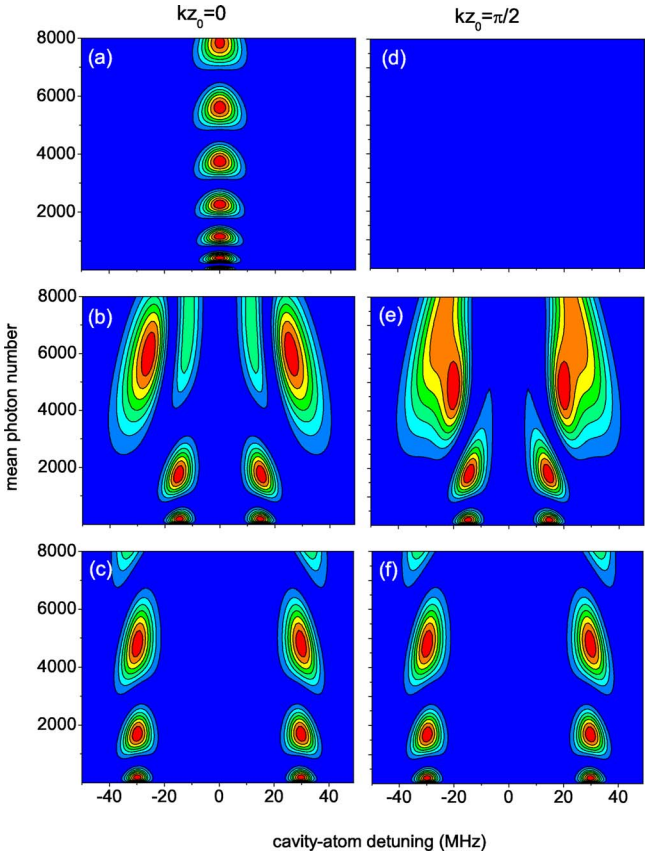

FIG. 5. (Color online) Density plots of P_{em} for a Gaussian mode profile. The same parameters and plot conventions are used as in Fig. 4. From the first row to the third $\delta/2\pi$ are 0, 15, and 30 MHz, respectively.

As the tilt angle gets larger, the similarity between two cases or the uniformity of interaction reaches the higher branch solutions. In the regime where the spatially uniform coupling is achieved, the Rabi frequency is effectively reduced to a half of its maximum value as it should be. This general behavior is also observed qualitatively with a realistic Gaussian mode function in the next section.

B. Gaussian mode profile

On resonance the mode profile does not matter if the integrated Rabi angles are set the same. At off resonance, however, the response of the atom is different. In terms of Bloch vector the torque vector $[\Omega(t),0,\Delta]$ is fixed for the top-hat profile, while the torque vector wobbles due to the adiabatic variation in Rabi frequency as a function of time for the time-varying envelope. The results for a Gaussian TEM_{00} mode are shown in Fig. 5. The overall tendency is the same as in the case of top hat except that the degree of kz_0 dependence is somewhat reduced. We ascribe it to the fact that the adiabatic nature of Gaussian envelope suppresses the spurious harmonic resonances, which is induced by the square edges of the top-hat profile. For intermediate tilt angles, for which $\delta \sim \sqrt{n}g$ for the third branch solution as in (b) and (e), the frequency pushing is evident due to the harmonic resonances. For larger tilt angles as in (c) and (f) clean Rabi oscillations are recovered.

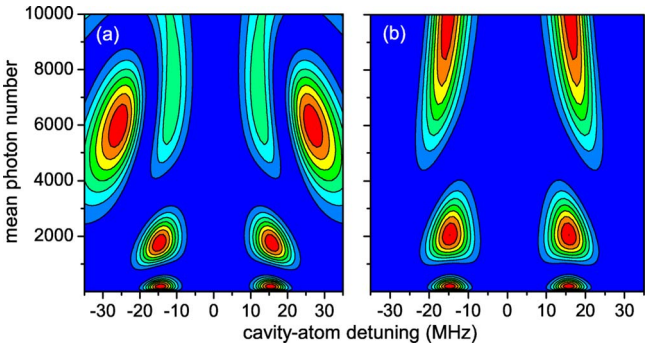

FIG. 6. (Color online) Density plots of P_{em} for $\delta/2\pi = 15$ MHz at $kz_0=0$. (a) By the exact calculation and (b) by the approximate calculation of Ref. [11].

As mentioned earlier the validity of decomposing the atomic polarization into two traveling-wave components as in Ref. [11] is limited to small λ. Consequently, the interference effect or the frequency-pushing effect is more pronounced in the third branch for the exact calculation than the approximation of Ref. [11] as shown in Fig. 6.

V. EXPERIMENTAL TEST OF THEORY

To verify the validity of our theory we conducted the same type of experiment as in Ref. [9]. With a high enough atomic flux of mean velocity 800 m/s and inhomogeneous velocity width of 30% [full width at half maximum (FWHM)], we could observe the microlaser signal corresponding up to the third branch solution. The detuning curves were measured for two different tilt angles. In Fig. 7, $\delta/2\pi=15$ MHz in (a) and $\delta/2\pi=35$ MHz in (b) so that $\delta/(\sqrt{n_{\max}}g)\sim 1$ and 2.4, respectively, where $n_{\max}$ is the maximal mean photon number involved. In the experiment of Ref. [9], $\delta/(\sqrt{n_{\max}}g)$ was about 0.9, close to the situation in (a). The frequency pushing, which manifests itself for intermediate tilt angles or Doppler shifts ($\delta \sim \sqrt{n}g$), disappears for the large enough Doppler shift as expected. In the latter case, the detuning curve is more or less symmetric about each Doppler-shifted resonance, implying spatially uniform atom-cavity interactions.

The level of each branch solution and the shift of resonance are in a good agreement with a theoretical fit with the mean atom number as a fitting parameter. The reason why the atom number is a fitting parameter is a practical one, namely, the atomic flux may vary in experiments depending on the tilt angle due to screening by a collimating aperture along the path of the atomic beam.

Although the branch solutions are disconnected to one another, the observed mean photon number jumps from one branch to another at specific detunings. Even hysteresis is observed with respect to the cavity scanning direction [9]. This phenomena, now under study, can be understood qualitatively in terms of Fokker-Planck analysis of quantum tunneling between the double-well potentials [10]. The reason

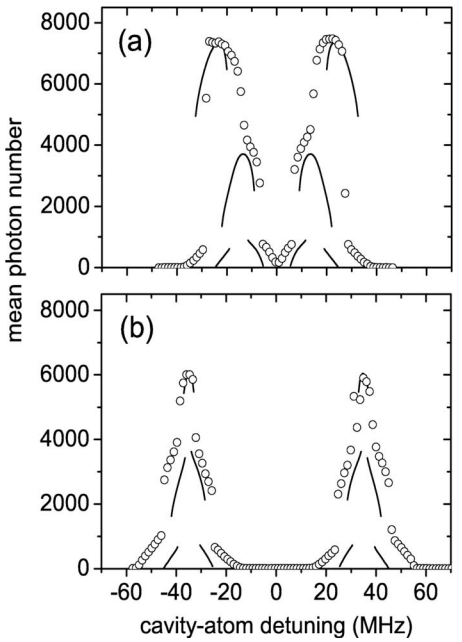

FIG. 7. Detuning curves for (a) $\delta/2\pi=15$ MHz and (b) $\delta/2\pi=35$ MHz. Circle: experiments, line: theoretical curves which are obtained for the mean intracavity atom number of $N=800$ in (a) and $N=900$ in (b).

for additional broadening which occurs when each branch solution approaches a saturation region is still not known and will be investigated in the future.

VI. CONCLUSION

We have shown that the interference between the atomic dipoles induced by two traveling-wave components brings about the frequency-pushing effect observed in the detuning curve of the cavity-QED microlaser. This interference is the very mechanism that prevents us from achieving the spatially uniform atom-cavity interactions when deliberately tilting the atomic beam. Our analysis is done by evaluating the unitary operator associated with the atom-cavity interaction in Dyson series with an explicit time-position-dependent atom-cavity coupling. Analytic explanations are given to understand the numerical and the experimental results. The criteria for achieving the uniform atom-cavity interaction is to set the Doppler shift by tilting the atomic beam much larger than both the inverse of transit time and the accumulated Rabi frequency involved. We found that the observed third branch deviating from the prediction of uniform coupling theory in the experiment of Ref. [9] is due to the Doppler shift not large enough compared to the Rabi frequency associated with the third branch. Almost symmetric detuning curve was obtained in an experiment with a larger Doppler shift, implying a spatially uniform coupling was achieved there.

ACKNOWLEDGMENTS

This work was supported by National Research Laboratory, KRF (Grant No. 2005-070-C00058), and WCU Grant.

[1] D. Meschede, H. Walther, and G. Muller, Phys. Rev. Lett. **54**, 551 (1985).
[2] K. An, J. J. Childs, R. R. Dasari, and M. S. Feld, Phys. Rev. Lett. **73**, 3375 (1994).
[3] G. Rempe, R. J. Thompson, R. J. Brecha, W. D. Lee, and H. J. Kimble, Phys. Rev. Lett. **67**, 1727 (1991).
[4] R. J. Thompson, G. Rempe, and H. J. Kimble, Phys. Rev. Lett. **68**, 1132 (1992).
[5] J. J. Childs, K. An, M. S. Otteson, R. R. Dasari, and M. S. Feld, Phys. Rev. Lett. **77**, 2901 (1996).
[6] G. T. Foster, L. A. Orozco, H. M. Castro-Beltran, and H. J. Carmichael, Phys. Rev. Lett. **85**, 3149 (2000).
[7] K. An, R. R. Dasari, and M. S. Feld, Opt. Lett. **22**, 1500 (1997).
[8] W. Choi, J.-H. Lee, K. An, C. Fang-Yen, R. R. Dasari, and M. S. Feld, Phys. Rev. Lett. **96**, 093603 (2006).
[9] C. Fang-Yen, C. C. Yu, S. Ha, W. Choi, K. An, R. R. Dasari, and M. S. Feld, Phys. Rev. A **73**, 041802(R) (2006).
[10] C. Fang-Yen, Ph.D. thesis, Massachusetts Institute of Technology, 2002.
[11] K. An, J. Korean Phys. Soc. **42**, 505 (2003).
[12] R. E. Silverans, G. Borghs, P. De Bisschop, and M. Van Hove, Phys. Rev. Lett. **55**, 1070 (1985).
[13] J. H. Eberly and V. D. Popov, Phys. Rev. A **37**, 2012 (1988).
[14] S. P. Goreslavsky and V. D. Popov, Phys. Rev. A **39**, 2228 (1989).
[15] T. W. Mossberg and M. Lewenstein, Phys. Rev. A **39**, 163 (1989).
[16] K. An, Y. T. Chough, and S. H. Youn, Phys. Rev. A **62**, 023819 (2000).
[17] L. Horvath and H. J. Carmichael, Phys. Rev. A **76**, 043821 (2007).
[18] P. Filipowicz, J. Javanainen, and P. Meystre, Phys. Rev. A **34**, 3077 (1986).
[19] K. An, J. Phys. Soc. Jpn. **72**, 811 (2003).
[20] M. O. Scully and M. S. Zubairy, *Quantum Optics* (Cambridge University Press, Cambridge, 1997).